Int. J. Electron. Commun. (AEÜ) 84 (2018) 321–330

Contents lists available at ScienceDirect

Int. J. Electron. Commun. (AEÜ)

journal homepage: www.elsevier.com/locate/aeue

Regular paper

DOA error estimation in 3D cylindrical dipole array geometries including the mutual coupling effect

Sarah Poormohammad, Zahra Sasan Nia, Forouhar Farzaneh*

Department of Electrical Engineering, Sharif University of Technology, Tehran 11155-4363, Iran

ARTICLE INFO

Keywords:
Array geometry
Rotated-cylindrical geometry
DOA
MUSIC
Mutual coupling
3D dipole array
Monte-Carlo simulation

ABSTRACT

The direction of arrival (DOA) error in dipole 3D arrays is estimated through Monte-Carlo simulations using the standard MUSIC algorithm. Novel 3D geometries are implemented which demonstrate better precision given the same lateral area. The mutual coupling effect is included by changing the search vector in the MUSIC DOA algorithm for the novel 3D geometries. A simple straight forward method is used which does not need complex electromagnetic computations. Simulations show that the proposed method can successfully account for the mutual coupling effects in two dimensional direction finding (both azimuth and elevation angle) with novel 3D array geometries. Reduced DOA estimation error is observed in the novel geometries which can be used as a method of mitigation for the mutual coupling effect.

1. Introduction

In the past decades different DOA estimation algorithms have been evaluated and examined for 1-D and 2-D smart antenna arrays. Some of these algorithms such as MUSIC and ESPRIT showed accurate and stable performances in azimuth or azimuth/elevation estimations with different numbers of snapshots and SNR values [1]. In practical cases where the mutual coupling between antenna elements or scattering effects of the environment are significant, most DOA estimation algorithms failed to predict the angle of arrival for numerous sources correctly. Different studies were conducted to compute the effect of mutual coupling on the DOA estimation algorithms. In one of the initial studies in [2] the authors considered the effect of mutual coupling on the performance of adaptive arrays and used a deterministic solution to obtain the steering vector required to maximize the output SINR (Signal to Interference and Noise Ratio). In [3] the effect of mutual coupling in the linear arrays with 1-D (elevation only) MUSIC direction finding method was eliminated by changing the search vector. In [4] the authors developed an eigenstructure based algorithm for direction finding and calibration of the array parameters. In [5] the mutual coupling effect was considered by an electromagnetic computation method for both Bartlett and MUSIC direction of arrival estimations. In [6] authors used the method of [5] for MUSIC direction of arrival estimation with circular array configuration. Another comparative study between the performance of MUSIC and Bartlett DOA estimations which considered the mutual coupling effects of physical dipole antenna arrays with impedance matrix was conducted in [7] and the authors showed that the MUSIC direction finding has a more accurate angular estimation than the Bartlett algorithm. In [8] Method of Moment (MoM) was used to characterize the antenna array for considering the mutual coupling effect. In [9] a new method for the calculation of mutual impedances based on an estimated current distribution was introduced. In [10] a blind calibration method was used for the mutual coupling effect and DOA estimation and it showed that the Uniform Circular Array (UCA) has some advantages compared to Uniform Linear Array (ULA) in wideband applications.

As mentioned above many different methods were proposed for 1-D (elevation only) direction of arrival estimations in the presence of mutual coupling between elements of the array. Most of these solutions were based on the ULA or UCA or URA (Uniform Rectangular Array) configurations of antennas for azimuth or elevation estimation. Some methods were introduced for both azimuth and elevation estimations in [11–13]. Effect of mutual coupling on the 2-D (azimuth and elevation) MUSIC algorithm with MoM matrix method was compensated in [11]. Combining the uniform circular array-RAnk REduction (UCA-RARE) and Root-MUSIC algorithm for 2-D (azimuth and elevation) direction of arrival (DOA) estimation for uniform circular arrays in the presence of mutual coupling was examined in [12]. In [13] the authors used auxiliary sensors on the boundary of Uniform Rectangular Array (URA) to estimate accurate DOA for elevation and azimuth angles and mutual coupling without any calibration or iterative procedure. In [14] a Modified Root-MUSIC algorithm is proposed to estimate the angle of arrival and the polarization of the plane waves with diversely polarized uniform circular array (UCA) in the presence of mutual coupling effects

* Corresponding author.
E-mail address: farzaneh@sharif.edu (F. Farzaneh).

https://doi.org/10.1016/j.aeue.2017.12.019
Received 4 July 2017; Accepted 17 December 2017

between the antenna arrays. Another algorithm which modifies the beam space for 2D DOA estimation in the presence of mutual coupling effect, with a small number of elements in UCA configuration was proposed in [15]. Improving the accuracy of both azimuth and elevation angles estimation in the presence of mutual coupling is still an open area for the researchers. Considering the mutual coupling effect between the elements of 3D antenna geometries employing 2-D (azimuth and elevation) MUSIC direction finding algorithm is a new issue for DOA estimations. In this paper we employ the basic formulation of [3] which is based on the MUSIC direction finding algorithm for compensation of mutual coupling effects between the elements of the arrays for a number of 3D array geometries, namely 3D circular array, 3D triangular array and 3D rotated circular array and 3D rotated triangular array of half-wave dipole antennas for joint azimuth and elevation angles estimation. These novel geometries were introduced in [16] and Monte-Carlo simulations showed that the rotated cross section 3D arrays demonstrated lower error estimation than the normal 3D arrays without accounting for the mutual coupling effect. We employ some of these novel geometries with two-layer and three-layer configurations using the direction finding MUSIC algorithm with mutual coupling effect included, to achieve a more realistic error estimation.

Incident signals are assumed to be uncorrelated sources and Monte-Carlo simulations are conducted to compare the RMSE (Root Mean Square Error) of the arrival angles for different configurations. This study investigates the effect of array geometry (2D and 3D arrays) on the accuracy of azimuth and elevation angles estimation in presence of mutual coupling effects based on the extension of the method used in [3]. It has been demonstrated that with this approach MUSIC algorithm can be utilized for both azimuth and elevation angles estimation with sufficient accuracy in presence of mutual coupling among the elements. Monte-Carlo simulation shows that the proposed method for azimuth and elevation angles estimation with 3D array configuration achieves a good resolution in comparison to other geometries [16]. This method does not need the complex time consuming numerical electromagnetic computations. Furthermore the introduction of the new rotated array geometries including two-layer and three-layer triangular arrays provide better resolution in comparison to the conventional arrays, in the presence of mutual coupling.

This paper is divided into four sections. Section 2 presents the data model for proposed arrays in presence of mutual coupling effect between dipole antennas. Section 3 represents the comparison of 3D circular and 3D triangular geometries' performances with equal lateral areas using physical dipole elements. Finally Section 4 draws the conclusion.

2. Data model for proposed arrays in presence of mutual coupling

Two dimensional arrays such as circular arrays can estimate azimuth angles with a high resolution while they have less accuracy in estimating elevation angles with respect to three dimensional arrays. For this reason the three dimensional arrays are proposed. Typical three dimensional cylindrical arrays like 3D circular and 3D triangular with 36 elements are shown in Fig. 1a and b. These arrays contain isotropic elements. So the radiation pattern can be described by the array factor. In order to obtain the array model and estimate the azimuth/elevation angles of arrival by MUSIC algorithm, the first step is to find the array steering vector $\boldsymbol{a}(\theta, \varphi)$ for isotropic elements [16].

$$\boldsymbol{a}(\theta,\varphi) = e^{-j\boldsymbol{PK}} \tag{1}$$

where $\boldsymbol{P}$ is the position matrix of array elements and $\boldsymbol{K}$ is the wave number matrix.

In this study, three dimensional arrays contain M planes of circular or triangular arrays and each array consists of N elements. So the wave number matrix is defined by:

$$\boldsymbol{K} = [\boldsymbol{k}_C\ \boldsymbol{k}_C\ \ldots\ \boldsymbol{k}_C]^T_{(3M)\times 1} \tag{2}$$

where $\boldsymbol{k}_C$ is the wave vector and T superscript stands for transpose matrix.

$$\boldsymbol{k}_C = \frac{2\pi}{\lambda}[\sin\theta\cos\varphi\ \sin\theta\sin\varphi\ \cos\theta] \tag{3}$$

where λ is the operating wave-length and the position matrix of the array elements is given by:

$$\boldsymbol{P} = [\boldsymbol{r}_x\ \boldsymbol{r}_y\ \boldsymbol{z}_1,\ \boldsymbol{r}_x\ \boldsymbol{r}_y\ \boldsymbol{z}_2,\ \ldots,\ \boldsymbol{r}_x\ \boldsymbol{r}_y\ \boldsymbol{z}_M]_{N\times(3M)} \tag{4}$$

where $\boldsymbol{r}_x$, $\boldsymbol{r}_y$ and $\boldsymbol{z}_m$ are the position of mth circular array elements on x-axis, y-axis and z-axis respectively. For example, in the circular configuration case which is centered at the origin the position of elements are given as below.

$$\boldsymbol{r}_x = R[\cos\varphi_1\ \cos\varphi_2\ \ldots\ \cos\varphi_N]^T_{N\times 1} \tag{5}$$

$$\boldsymbol{r}_y = R[\sin\varphi_1\ \sin\varphi_2\ \ldots\ \sin\varphi_N]^T_{N\times 1} \tag{6}$$

$$\boldsymbol{z}_m = h_m[1\ 1\ \ldots\ 1]^T_{N\times 1} \tag{7}$$

In the above equations, R is the radius of each circular array, $\varphi_n = \frac{2\pi}{N}(n-1), n = 1,2,\ldots,N$ and () is the height of the mth plane. By substituting Eqs. (5)–(7) in (4), the position matrix ($\boldsymbol{P}$) in circular configuration can be written as:

$$\boldsymbol{P} = \begin{bmatrix} R\cos\varphi_1 & R\sin\varphi_1 & h_1 & R\cos\varphi_1 & R\sin\varphi_1 & h_2 & \ldots & R\cos\varphi_1 & R\sin\varphi_1 & h_M \\ R\cos\varphi_2 & R\sin\varphi_2 & h_1 & R\cos\varphi_2 & R\sin\varphi_2 & h_2 & & R\cos\varphi_2 & R\sin\varphi_2 & h_M \\ \vdots & \vdots & \vdots & \vdots & \vdots & \vdots & & \vdots & \vdots & \vdots \\ R\cos\varphi_N & R\sin\varphi_N & h_1 & R\cos\varphi_N & R\sin\varphi_N & h_2 & & R\cos\varphi_N & R\sin\varphi_N & h_M \end{bmatrix}_{N\times(3M)} \tag{8}$$

So the array steering vector is obtained as,

$$\boldsymbol{a}(\theta,\varphi) = \begin{bmatrix} e^{j\frac{2\pi}{\lambda}[MR\sin\theta\cos(\varphi-\varphi_1)+(h_1+h_2+\cdots+h_M)\cos\theta]} \\ e^{j\frac{2\pi}{\lambda}[MR\sin\theta\cos(\varphi-\varphi_2)+(h_1+h_2+\cdots+h_M)\cos\theta]} \\ \vdots \\ e^{j\frac{2\pi}{\lambda}[MR\sin\theta\cos(\varphi-\varphi_N)+(h_1+h_2+\cdots+h_M)\cos\theta]} \end{bmatrix}_{N\times 1} \tag{9}$$

For the triangular configuration one can compute $\boldsymbol{r}_x$, $\boldsymbol{r}_y$ and z_m of mth element of triangular array in the cartesian coordinates system and replace it as the position vector in Eqs. (7)–(9) respectively. If the process $\boldsymbol{x}$ is ergodic, the array correlation matrix can be computed by Eq. (10).

$$\boldsymbol{R}_{xx} \approx \frac{1}{K}\sum_{k=1}^{K} \boldsymbol{x}(k)\boldsymbol{x}^H \tag{10}$$

Where H superscript stands for the Hermitian vector and

$$\boldsymbol{x}(k) = [\boldsymbol{a}(\theta_1,\varphi_1),\ \boldsymbol{a}(\theta_2,\varphi_2),\ \ldots,\ \boldsymbol{a}(\theta_D,\varphi_D)]\begin{bmatrix} s_1(k) \\ s_2(k) \\ \vdots \\ s_D(k) \end{bmatrix} + \boldsymbol{n}(k) = \boldsymbol{A}\boldsymbol{s}(k) + \boldsymbol{n}(k) \tag{11}$$

In (11), $\mathbf{A}$ is the matrix of steering vectors, $\boldsymbol{s}(k)$ is the vector of incident signals at the kth snapshot, $\boldsymbol{n}(k)$ is the noise vector at the kth snapshot and D is the number of incident signals. So the MUSIC pseudospectrum is obtained as [1],

$$P_{MUSIC}(\theta,\varphi) = \frac{1}{|[\boldsymbol{a}^H(\theta,\varphi)\boldsymbol{E}_n\boldsymbol{E}_n^H\boldsymbol{a}(\theta,\varphi)]|} \tag{12}$$

where $\boldsymbol{E}_n$ is the noise subspace of the array correlation matrix. Eqs. (10)–(12) present the MUSIC pseudospectrum in the ideal situation with arrays of isotropic elements. As a realistic situation, we use half-wave dipole antennas in the array structures and consider the mutual coupling between antennas by expanding the method employed in [3] for two-plane and three-plane of circular and triangular arrays and their corresponding rotated cross section counterparts when the incident signals are uncorrelated.

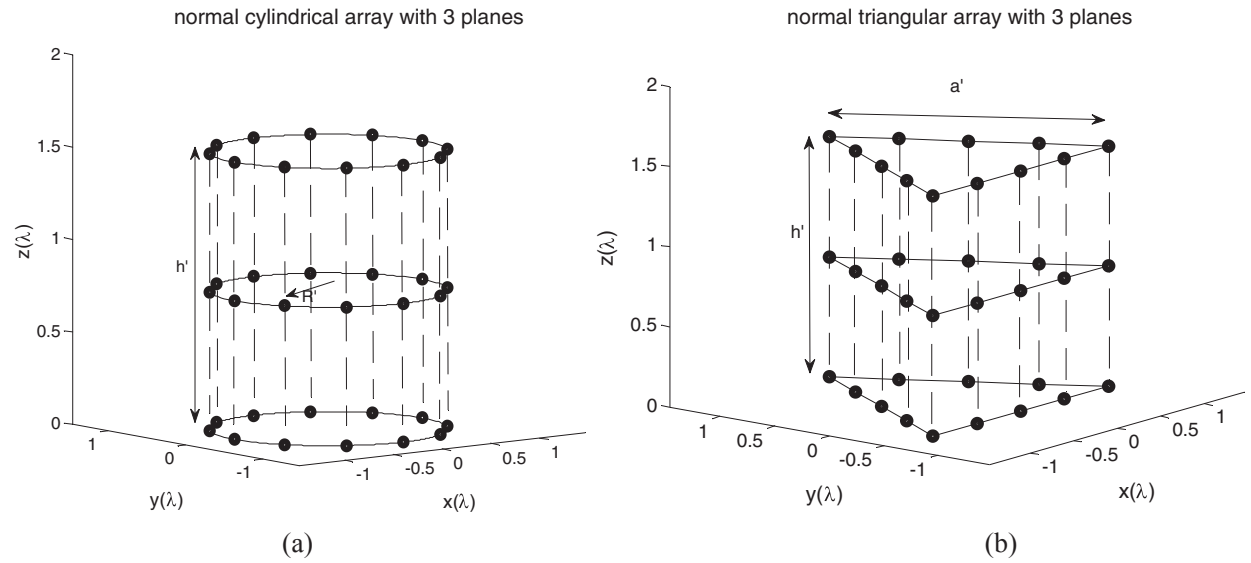

Fig. 1. 3D cylindrical arrays of isotropic elements. (a) Cylindrical array with circular cross section. (b) Cylindrical array with triangular cross section.

Once using real antennas in array structures, the amplitude of the steering vector is multiplied by the pattern factor of the antenna. The pattern factor for a half-wave dipole antenna, parallel to z-axis, is computed from (13) [17].

$$F(\theta) = \frac{\cos\left[\left(\frac{\pi}{2}\right)\cos\theta\right]}{\sin\theta} \tag{13}$$

So the array steering vector in this real situation becomes:

$$\boldsymbol{a}(\theta,\varphi) = \frac{\cos\left[\left(\frac{\pi}{2}\right)\cos\theta\right]}{\sin\theta}\boldsymbol{a}_i(\theta,\varphi) \tag{14}$$

where $\boldsymbol{a}_i(\theta,\varphi)$ is the array steering vector in ideal situation (isotropic elements) and $\boldsymbol{a}(\theta,\varphi)$ is the array steering vector in new situation. Note that using dipole antennas in the array structure makes the search function to approach infinity, remind relations (12) and (14), where the pattern factor becomes zero and in a physical array one cannot estimate the signal DOA's located at the element's zenith.

In order to compute the pseudospectrum in the MUSIC algorithm in real situation, the vector of signals received at the array elements at the kth snapshot is [3]:

$$\boldsymbol{x}(k) = \boldsymbol{Z}_0^{-1}\boldsymbol{A}\boldsymbol{s}(k) + \boldsymbol{n}(k) \tag{15}$$

where $\boldsymbol{Z}_0$ is the normalized impedance matrix [3], $\boldsymbol{A}$ is the matrix of steering vectors, $\boldsymbol{s}(k)$ and $\boldsymbol{n}(k)$ are the source and noise vectors at the kth snapshot respectively. The array correlation matrix in a real situation is given as:

$$\boldsymbol{R}_{\boldsymbol{xx}} = E[\boldsymbol{x}\ \boldsymbol{x}^H] = (\boldsymbol{Z}_0^{-1}\boldsymbol{A})\boldsymbol{R}_{SS}(\boldsymbol{Z}_0^{-1}\boldsymbol{A})^H + \boldsymbol{R}_{nn} \tag{16}$$

where $\boldsymbol{R}_{SS}$ and $\boldsymbol{R}_{nn}$ are the source and the noise correlation matrices respectively. So the search function (pseudospectrum) of MUSIC method can be formed as (17) to include the mutual coupling effects.

$$P_{MUSIC}(\theta,\varphi) = \frac{1}{|\boldsymbol{a}^{\boldsymbol{H}}(\theta,\varphi)(\boldsymbol{Z}_0^{-1})^{\boldsymbol{H}}\boldsymbol{E}_n\boldsymbol{E}_n^H(\boldsymbol{Z}_0^{-1})\boldsymbol{a}(\theta,\varphi)|} \tag{17}$$

Or in a simpler form:

$$P_{MUSIC}(\theta,\varphi) = \frac{1}{|\boldsymbol{E}_n^H\boldsymbol{Z}_0^{-1}\boldsymbol{a}(\theta,\varphi)|^2} \tag{18}$$

In the above equation, $\boldsymbol{Z}_0$ is defined as [3]:

$$\boldsymbol{Z}_0 = \begin{bmatrix} 1+\frac{Z_{11}}{Z_L} & \frac{Z_{12}}{Z_L} & \dots & \frac{Z_{1N}}{Z_L} \\ \frac{Z_{21}}{Z_L} & 1+\frac{Z_{22}}{Z_L} & \dots & \frac{Z_{2N}}{Z_L} \\ \vdots & \vdots & \vdots & \vdots \\ \frac{Z_{N1}}{Z_L} & \frac{Z_{N2}}{Z_L} & \dots & 1+\frac{Z_{NN}}{Z_L} \end{bmatrix} \tag{19}$$

where the Z_{nn} are the self-impedance and the Z_{nl} are the mutual impedance between antennas and Z_L is the load impedance.

The self-impedance of a half-wave dipole antenna is [17]:

$$\begin{aligned} Z_{nn} = R_{nn} + jX_{nn} &= 30[0.577 + \ln(2\pi) - \mathrm{Ci}(2\pi)] + j30\mathrm{Si}(2\pi) \\ &= 73.2 + j42.5\ (\Omega) \end{aligned} \tag{20}$$

There are three arrangements for two parallel antennas as shown in Fig. 2a to c. The dipole antenna elements in the proposed configurations, from the mutual coupling point of view, may be in three arrangements, side-by-side (e.g. element (1) and (2)), collinear (e.g. elements (1) and (3)) and in echelon (e.g. elements (1) and (4)) as in Fig. 2d.

The mutual-impedance of two parallel side-by-side antennas is obtained from (21) [17].

$$Z_{21} = R_{21} + jX_{21} = R_{12} + jX_{12} = Z_{12} \tag{21}$$

where

$$R_{21} = 30\{2\ \mathrm{Ci}(\beta d) - \mathrm{Ci}[\beta(\sqrt{d^2+L^2}+\mathrm{L})] - \mathrm{Ci}[\beta(\sqrt{d^2+L^2}-\mathrm{L})]\}\ (\Omega) \tag{22}$$

and

$$X_{21} = -30\{2\ \mathrm{Si}(\beta d) - \mathrm{Si}[\beta(\sqrt{d^2+L^2}+\mathrm{L})] - \mathrm{Si}[\beta(\sqrt{d^2+L^2}-\mathrm{L})]\}\ (\Omega) \tag{23}$$

In (22) and (23), $\beta = \frac{2\pi}{\lambda}$, $L = \frac{\lambda}{2}$, $\mathrm{Ci(x)} = -\int_x^\infty \frac{\cos(t)}{t}dt$ is the cosine integral and $\mathrm{Si(x)} = \int_0^x \frac{\sin(t)}{t}dt$ is the sine integral [17]. For collinear antennas, Z_{nl} is computed from (24) and (25) [17].

$$\begin{aligned} R_{21} = &-15\cos\beta h\left[-2\ \mathrm{Ci}\ 2\beta h + \mathrm{Ci}\ 2\beta(h-L) + \mathrm{Ci}\ 2\beta(h+L) - \ln\left(\frac{h^2-L^2}{h^2}\right)\right] \\ &+ 15\sin\beta h[2\ \mathrm{Si}\ 2\beta h - \mathrm{Si}\ 2\beta(h-L) - \mathrm{Si}\ 2\beta(h+L)]\ (\Omega) \end{aligned} \tag{24}$$

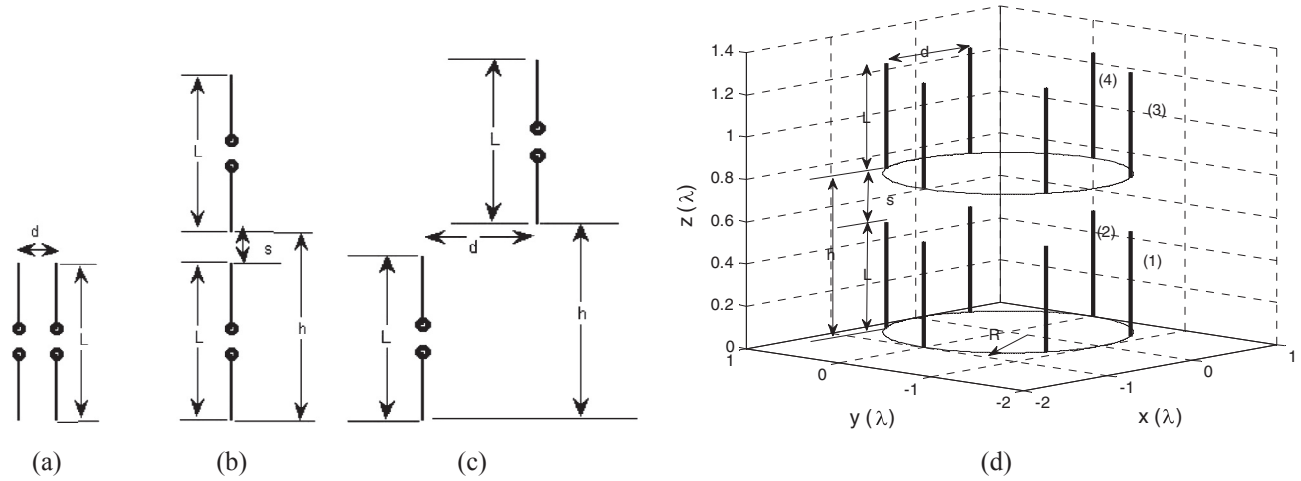

Fig. 2. Three arrangements of two parallel dipole antennas. (a) Side-by-side. (b) Collinear. (c) In echelon. (d) Typical cylindrical array showing the relative position of the antennas.

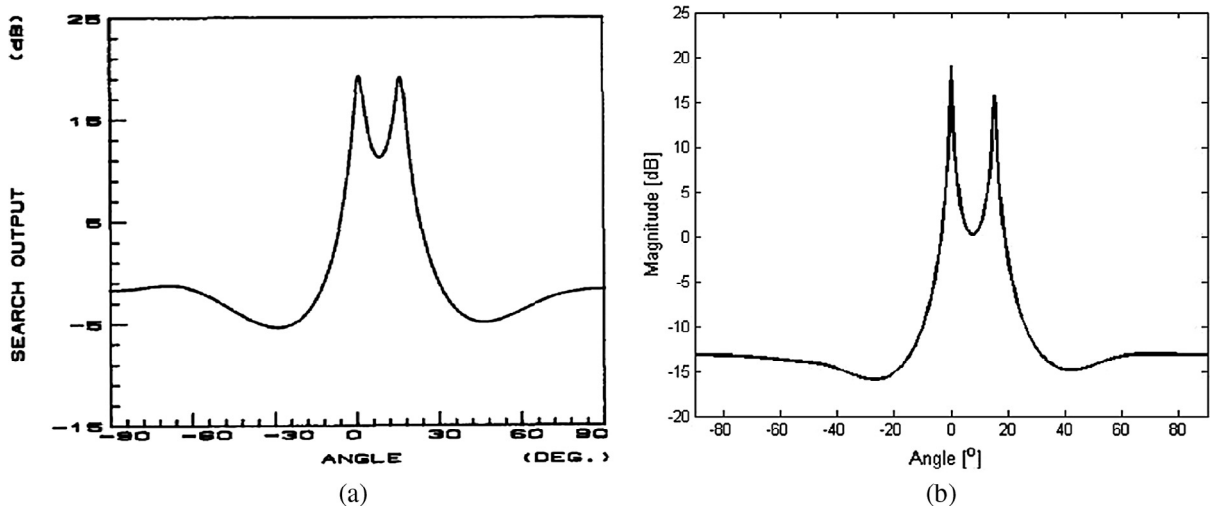

Fig. 3. Comparison of this work's MUSIC search function with that of Ref. [3]. (a) MUSIC search function in Ref. [3]. (b) MUSIC search function in this work.

$$X_{21} = -15\cos\beta h\,[2\ \mathrm{Si}\ 2\beta h - \mathrm{Si}\ 2\beta(h-L) - \mathrm{Si}\ 2\beta(h+L)] + 15\sin\beta h\,[2\mathrm{Ci}\ 2\beta h - \mathrm{Ci}\ 2\beta(h-L) - \mathrm{Ci}\ 2\beta(h+L) - \ln\left(\frac{h^2-L^2}{h^2}\right)]\ (\Omega) \tag{25}$$

For in echelon arrangements of antennas, Eqs. (26) and (27) are used [17].

$$R_{21} = -15\cos\beta h(-2\ \mathrm{Ci}\ A - 2\ \mathrm{Ci}\ A' + \mathrm{Ci}\ B + \mathrm{Ci}\ B' + \mathrm{Ci}\ C + \mathrm{Ci}\ C') + 15\sin\beta h(2\ \mathrm{Si}\ A - 2\ \mathrm{Si}\ A' - \mathrm{Si}\ B + \mathrm{Si}\ B' - \mathrm{Si}\ C + \mathrm{Si}\ C')\ (\Omega) \tag{26}$$

$$X_{21} = -15\cos\beta h(2\ \mathrm{Si}\ A + 2\ \mathrm{Si}\ A' - \mathrm{Si}\ B - \mathrm{Si}\ B' - \mathrm{Si}\ C - \mathrm{Si}\ C') + 15\sin\beta h(2\ \mathrm{Ci}\ A - 2\mathrm{Ci}\ A' - \mathrm{Ci}\ B + \mathrm{Ci}\ B' - \mathrm{Ci}\ C + \mathrm{Ci}\ C')\ (\Omega) \tag{27}$$

where

$$A = \beta(\sqrt{d^2+h^2} + h) \tag{28}$$

$$A' = \beta(\sqrt{d^2+h^2} - h) \tag{29}$$

$$B = \beta[\sqrt{d^2+(h-L)^2} + (h-L)] \tag{30}$$

$$B' = \beta[\sqrt{d^2+(h-L)^2} - (h-L)] \tag{31}$$

$$C = \beta[\sqrt{d^2+(h+L)^2} + (h+L)] \tag{32}$$

$$C' = \beta[\sqrt{d^2+(h+L)^2} - (h+L)] \tag{33}$$

In order to validate our model including the mutual coupling effect we compare our simulation with that mentioned in [3] for an equally spaced five-element half-wave dipole linear array with half-wavelength spacing. The load impedance is assumed to be the complex conjugate of the self-impedance of the antenna elements. Two sources located at 0° and 15° with equal power and 3 dB Signal to Noise Ratio (SNR) are used for simulations. The covariance matrix is computed from 300 samples. Fig. 3 shows our simulation in comparison with that of Ref. [3]. It can be seen that our simulation is quite close to that of reference's simulation, the difference being due to the fact that we have computed the pseudospectrum for 180 points while in Ref. [3] it has been computed for 36 points.

Furthermore to evaluate the RMSE performance, we have compared the method used in this paper with that of Ref. [10], where a configuration of 7-element uniform circular dipole array with a radius of 72 mm is considered. The authors in [10] have used a blind calibration method for considering the mutual coupling effect between the elements. The results of RMSE versus SNR for the signal incoming from 71° at 2.4 GHz with 50 Monte-Carlo simulations and 512 snapshots are compared to the values of RMSE in our simulations in Fig. 4.

Monte-Carlo simulation results in Fig. 4 demonstrate that the method used in this paper including mutual coupling effects has a very good agreement with those of [10].

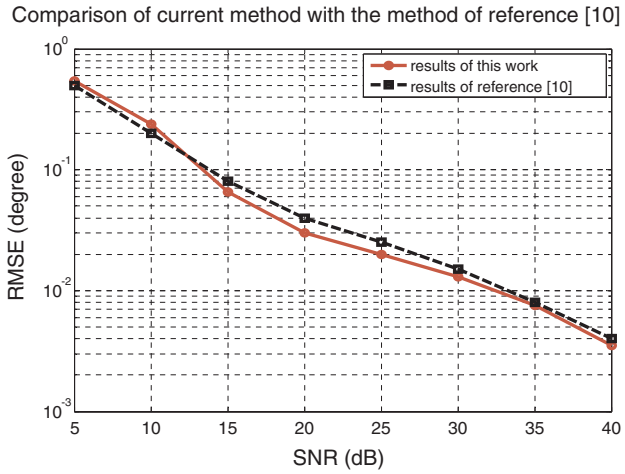

Fig. 4. Comparison of the simulation results of this work with those of [10] as a function of SNR for a 7-element UCA dipole array including the mutual coupling effect.

3. Comparison of different geometries, with equal lateral areas, in presence of mutual coupling

In this section, we compare different arrays including two-plane and three-plane geometries with circular and triangular normal cross sections and rotated cross sections with equal number of antennas and with equal lateral areas in a real situation (considering the mutual coupling between dipole antennas). If N_T is the total number of elements used in each array, the number of elements for each layer of two-layer array will be $N_T/2$ and for each layer of three-layer array will be $N_T/3$ and here N_T is 36 for all geometries. Two-layer circular array is shown in Fig. 5a and three-layer circular array is shown in Fig. 5b. For two-plane triangular array we place 18 elements for each plane of the two-layer array, equally spaced and for the three-plane triangular array 12 elements are equally spaced at each plane as in Fig. 5c and d.

We use three-plane array with circular cross sections including 12 elements in each plane and the elements in each planes of array are spaced by $\lambda/2$ as in Fig. 5b and therefore the radius of the circle of cross section (R') would be:

$$R' = \frac{\lambda/4}{\sin\left(\frac{\pi}{12}\right)} \tag{34}$$

In order to have equal lateral area in two-plane and three-plane arrays with circular cross sections, Eq. (35) should hold.

$$2\pi Rh = 2\pi R'h' \tag{35}$$

where R and R′ denote the radius of each circle in a two-plane antenna array and a three-plane antenna array respectively, and h and h′ denote the array heights as shown in Fig. 5a and b. We have chosen h= $\frac{3}{4}\lambda$,

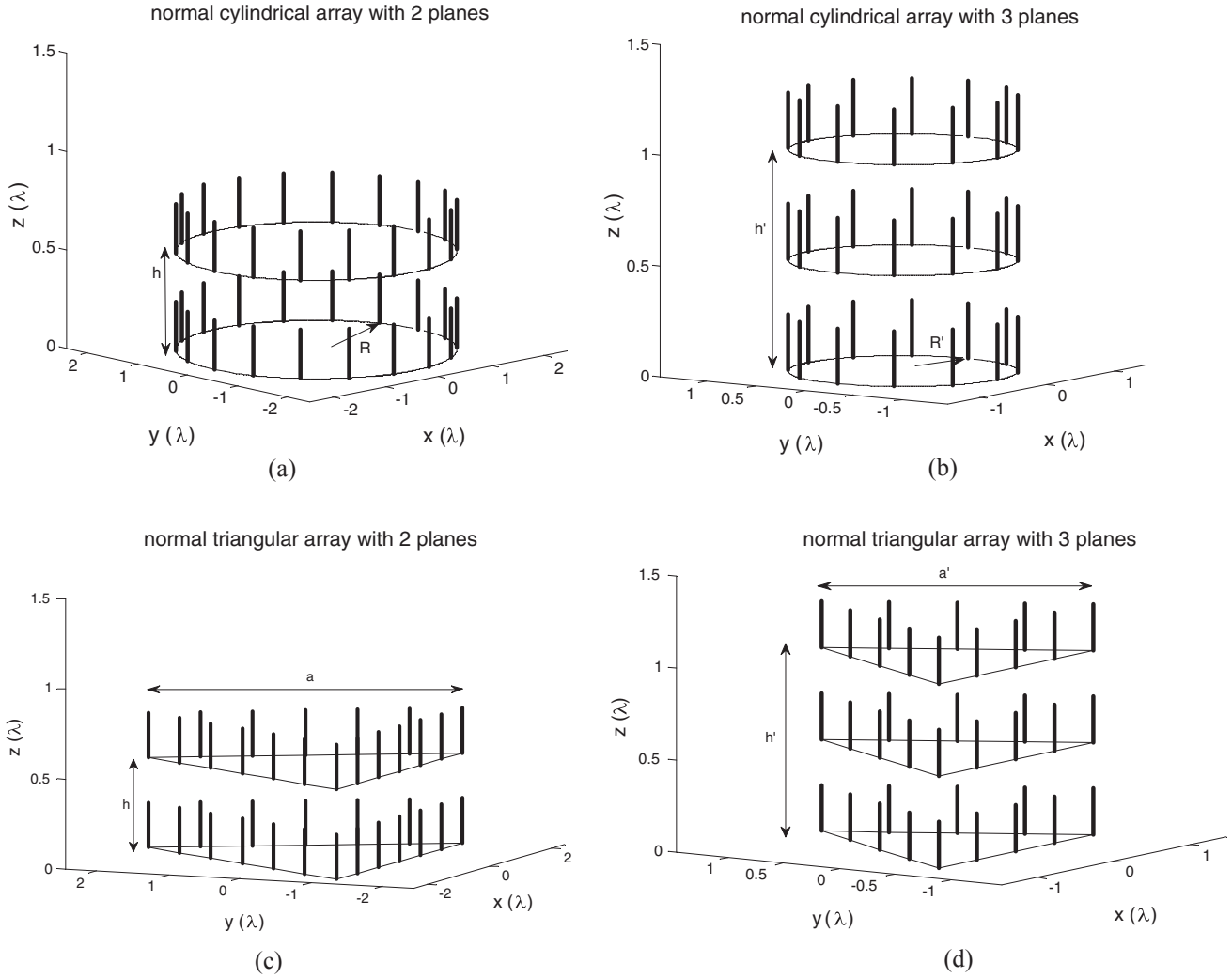

Fig. 5. Arrays of dipole antennas with circular cross sections and triangular cross sections and equal number of elements and equal lateral areas. (a) Two-layer circular array. (b) Three-layer circular array. (c) Two-layer triangular array. (d) Three-layer triangular array.

therefore $h' = \frac{3}{2}\lambda$ and R= 2R′. In order to have equal lateral area in two-plane triangular array and three-plane triangular array Eq. (36) should hold.

$$3ah = 3a'h' = 2\pi R'h' \tag{36}$$

where an and a′ denote the sides of the two-plane triangular array and three-plane triangular array respectively, and h and h' denote the array heights as shown in Fig. 5c and d. We have chosen $h = \frac{3}{4}\lambda$, therefore $h' = \frac{3}{2}\lambda$ and $a = 2a'$ and $a' = \frac{2\pi}{3}R'$.

We consider $R' = \frac{\lambda/4}{\sin(\frac{\pi}{12})}$, $h' = \frac{3}{2}\lambda$ for three-plane circular array and in the three remaining configurations the spacing between the elements is taken such that all the configurations would have the same lateral areas. All the geometries are centered about the origin in the xy plane. The RMSE of arrival angles is computed from Eq. (37).

$$RMSE = \sqrt{\frac{1}{2TN}\sum_{n=1}^{T}\sum_{i=1}^{Ns}[(\hat{\theta}_i^n - \theta_i^n)^2 + (\hat{\varphi}_i^n - \varphi_i^n)^2]} \tag{37}$$

where T and Ns are the number of random scenarios and the number of sources respectively. Furthermore $(\theta_i^n, \varphi_i^n)$ are the generated random angles of incidence of the sources and $(\hat{\theta}_i^n, \hat{\varphi}_i^n)$ are the estimated angle of arrivals. To begin, in order to evaluate the effect of mutual coupling in 3D arrays we can compare the RMSE for dipole cylindrical geometries of Fig. 5b and d with those of isotropic arrays (depicted in Fig. 1a and b) with equal lateral areas (with the same h′,R′ and a′). For this purpose we consider the number of uncorrelated signal sources Ns = 10 and the number of random scenarios T = 1200 (for elevation and azimuth incidence angles respectively with $\hat{\theta}_i^n \in [\pi/2, 3\pi/2]$ and $\hat{\varphi}_i^n \in [0, 2\pi]$). To estimate the RMSE versus the number of snapshots, our simulations are conducted by fixed signal to noise ratio (SNR = 7 dB) and varying number of snapshots from 20 to 200. The results of these Monte-Carlo simulations are shown in Fig. 6.

As it is observed in Fig. 6 considering the effect of mutual coupling the RMSE of the direction of arrival is increased roughly about 30% in each case (with the same geometry, the same area and the same number of elements). This shows the importance of the evaluation of the effect of the mutual coupling in DOA estimation.

We consider normal geometries (without rotated cross sections depicted in Fig. 5) and we examine the RMSE values including the mutual coupling effect between the half-wave dipole antennas to evaluate the precision of the method and the fitness of the geometries. To compare the mean values of RMSE for different geometries in presence of mutual coupling effect we can calculate the RMSE versus the number of snapshots and the signal to noise ratio (SNR). Again for this purpose we consider 10 uncorrelated signal sources and 1200 random scenarios. For calculation of the RMSE versus the number of snapshots in presence of mutual coupling effect, simulations are carried out at fixed SNR = 7 dB and varying snapshots between 20 and 200. Fig. 7a shows the RMSE versus number of snapshots in presence of mutual coupling effect for different geometries and the mean values of RMSE for each geometry is reported in Table 1.

As it is seen in Table 1 at fixed SNR and for equal number of antennas and equal lateral areas, triangular array with two planes has the lowest average RMSE for the estimated angles which is about 43% better than the circular array with three planes, in presence of mutual coupling effect. After comparing the RMSE, for different geometries, versus the number of snapshots as depicted in Fig. 7a, now we can compare the RMSE versus SNR for different geometries. Simulations were conducted for fixed number of snapshots (L = 100, where L is the number of snapshots) by varying the SNR between 0 and 14 dB. The number of sources were again taken as Ns = 10 and the number of random scenarios for azimuth and elevation incident angles were T = 1200. Fig. 7b shows the RMSE versus SNR for different array geometries, mutual coupling considered. The average of RMSE for estimation error of Fig. 7b is reported in Table 2 at fixed number of snapshots.

As it is observed in Fig. 7b for different array geometries, with equal lateral areas and equal number of antennas, at fixed number of snapshots, the triangular two-plane array has the lowest mean RMSE again which is about 45.5% better than the circular three-plane array and 13.5% better than the circular two-plane array. The results of Fig. 7a and b show that in presence of mutual coupling effect for equal lateral area geometries, 3D arrays with triangular cross sections have lower mean RMSE of estimation angles in comparison to 3D arrays with circular cross sections. The precision of triangular configuration for its lower estimation error has been also reported in [16] although there, isotropic antenna elements were employed without mutual coupling effect. It is noteworthy that in general the Monte-Carlo simulations, as

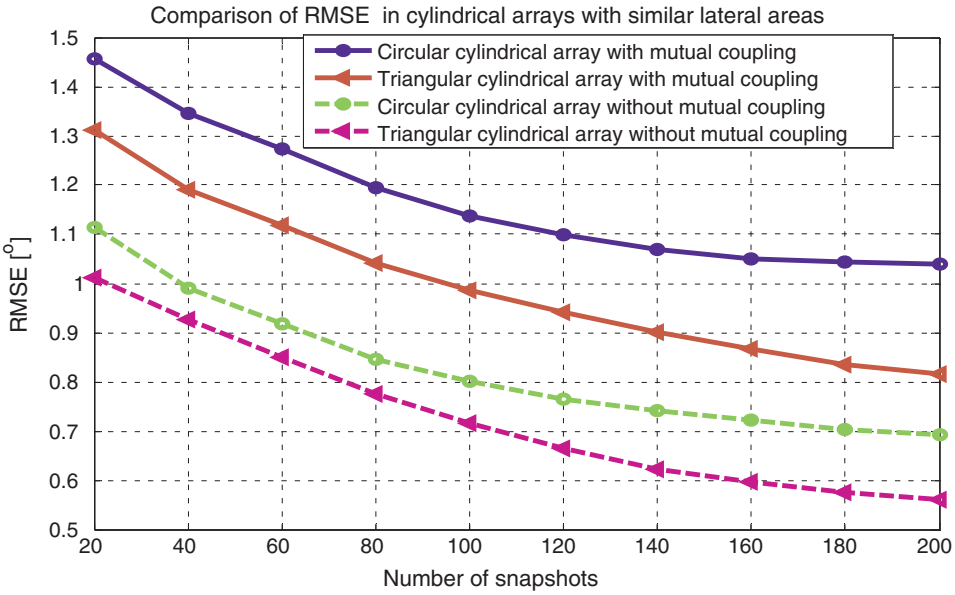

Fig. 6. Comparison of the RMSE versus the number of snapshots in cylindrical arrays of equal laetral areas and equal number of elements (at fixed SNR = 7 dB).

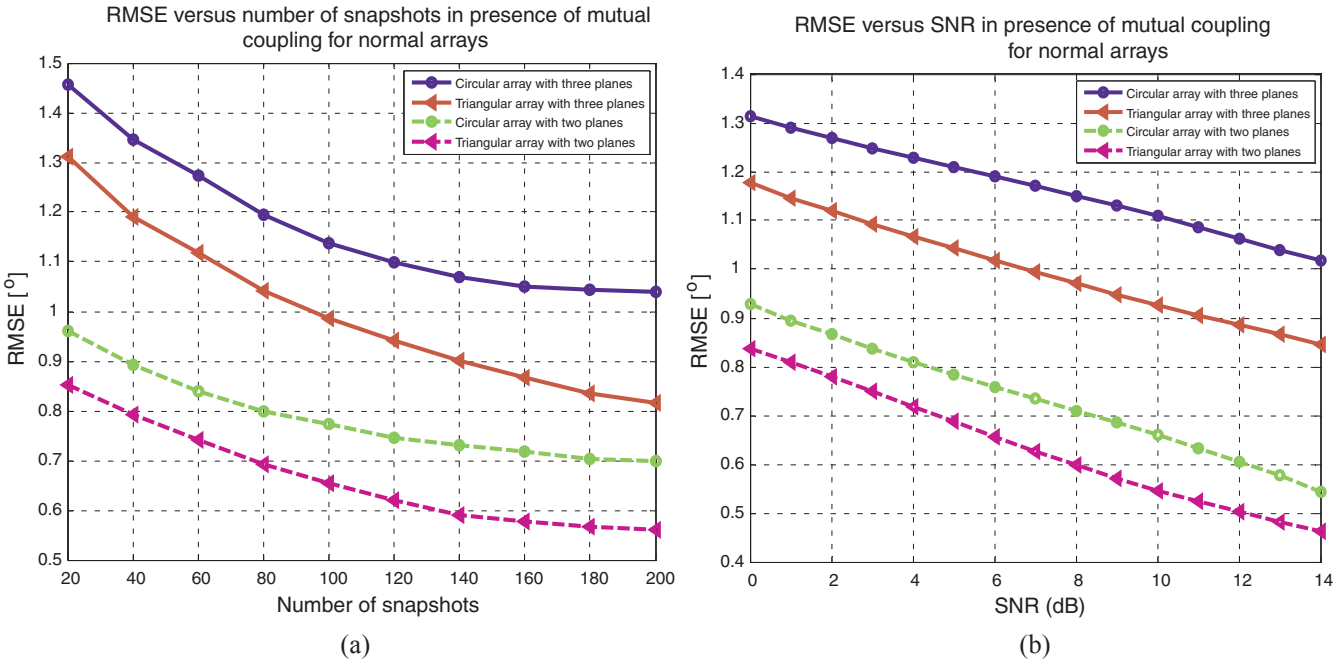

Fig. 7. Comparison of RMSE in different array geometries as a function of the number of snapshots and the SNR. (a) RMSE versus number of snapshots for different dipole array geometries with equal lateral areas (at fixed SNR = 7 dB). (b) RMSE versus SNR for different dipole array geometries with equal lateral areas (at fixed number of snapshots, L = 100).

in [16] with equal number of elements and equal number of sources at the same SNR, have lower RMSE than the simulations reported here. The reason is the inclusion of the mutual coupling effect in these simulations.

As it was stated in [16] employing novel 3D geometries with rotated cross sections have a significant effect on reducing the RMSE of the angle of arrival estimation. Let's evaluate the effect of the mutual coupling in the novel geometries presented in [16] to verify their superiority in a real situation as well. As shown in Fig. 8 for the two-plane arrays the rotation angle of the top plane is + φ_r about z-axis and the bottom plane is fixed, while for the three-plane arrays the rotation angle about z-axis is taken as + φ_r for the top plane and $-\varphi_r$ for the bottom plane and the middle plane is fixed. For the triangular cases φ_r was considered as 60° and for the circular cases φ_r was considered as10° for two-plane arrays and 15° for the three-plane arrays (indeed the rotation angle is considered as half the angular period). Rotated arrays with 36 dipole antennas for circular cross sections and triangular cross sections are shown in Fig. 8.

Now we conducted the Monte-Carlo simulations for computing the RMSE versus number of snapshots and SNR for rotated geometries including the mutual coupling effect between half-wave dipole antennas. The results of RMSE versus number of snapshots at fixed SNR = 7 dB, Ns = 10 and T = 1200 are shown in Fig. 9a for novel rotated geometries which were shown in Fig. 8 and the mean values of RMSE for each geometry are reported in Table 3.

If the RMSE simulations for novel rotated geometries are conducted at fixed number of snapshots (L = 100) and varying values of SNR between 0 and 14 dB with Ns = 10 and T = 1200 the results plotted in Fig. 9b will be obtained. The mean values of RMSE for novel rotated geometries at fixed SNR = 7 dB are reported in Table 4.

A comparison between the values of Table 1 with those of Table 3 shows that at fixed SNR the mean RMSE for angle of arrivals has improved about 21% for rotated circular array with three planes, 31% for rotated triangular array with three planes, 12% for rotated circular array with two planes and 41% for rotated triangular array with two planes with respect to the corresponding fixed arrays. For the fixed number of snapshots as shown in Tables 2 and 4 the mean RMSE for arrival angles has improved about 21% for the rotated circular array with three planes, 31% for the rotated triangular array with three planes, 19% for the rotated circular array with two planes and 37% for the rotated triangular array with two planes with respect to the corresponding fixed arrays of the same geometry. The results of simulations show that the mean RMSE of angle of arrivals including the mutual coupling effects can approach the mean RMSE of angle of arrivals for similar geometries of isotropic antenna elements (without coupling) when we employed the rotated geometries as introduced in [16] for direction finding. To demonstrate the superiority of rotated geometries with respect to normal geometries, the results of RMSE versus the number of snapshots and the SNR are plotted in Fig. 9c and d for triangular cross sections. As such we can employ the rotated geometries as a method of compensation for mitigating the effect of the mutual coupling.

Table 1
The average of estimation error for Fig. 7a.

Geometry	Average of estimation error (°)
Circular with three planes	1.162
Triangular with three planes	0.994
Circular with two planes	0.782
Triangular with two planes	0.661

Table 2
The average of estimation error for Fig. 7b.

Geometry	Average of estimation error (°)
Circular with three planes	1.168
Triangular with three planes	0.998
Circular with two planes	0.735
Triangular with two planes	0.636

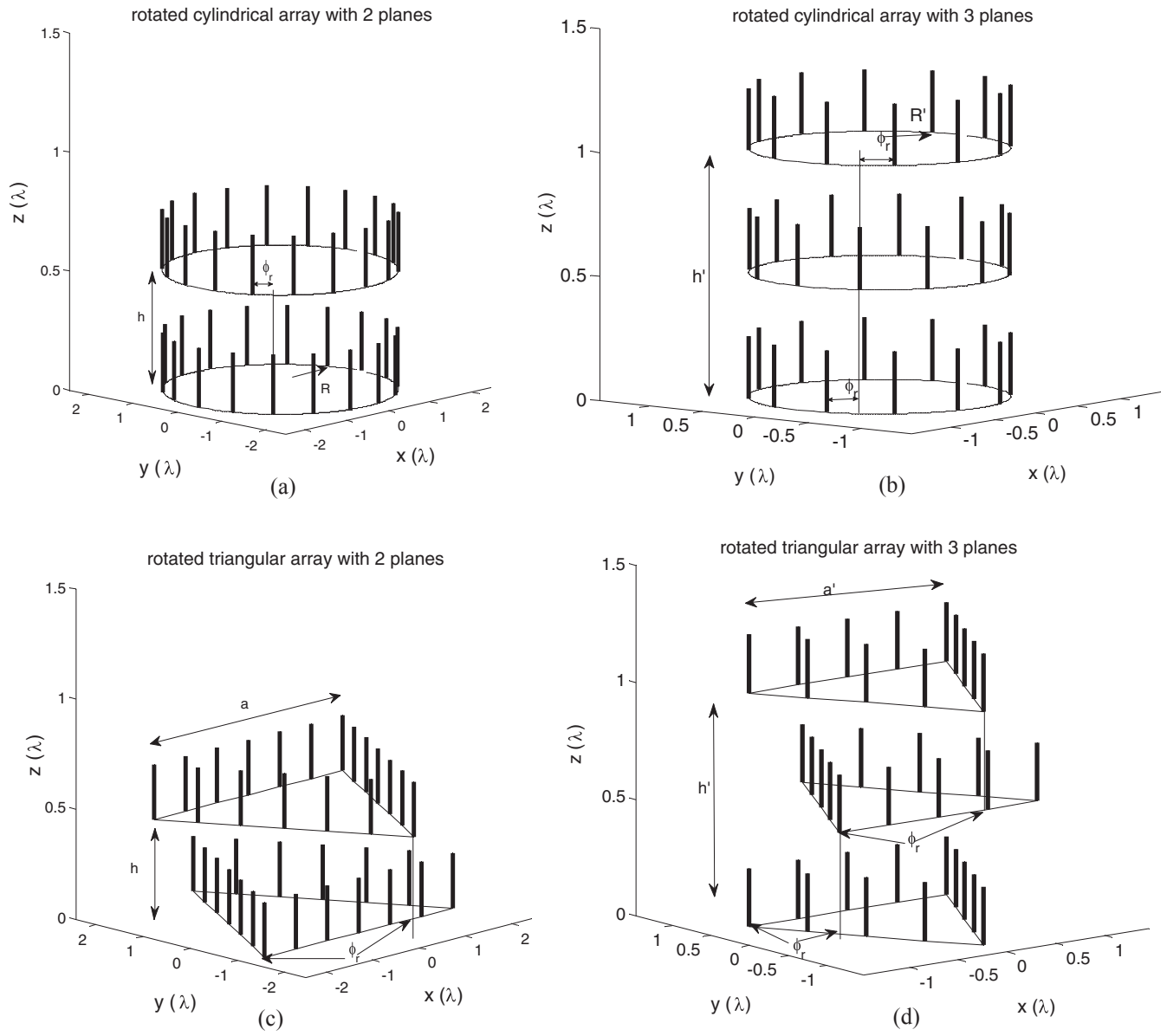

Fig. 8. Novel array geometries of dipole antennas with rotated cross sections and equal number of elements. (a) Rotated circular array with two layers. (b) Rotated circular array with three layers. (c) Rotated triangular array with two layers. (d) Rotated triangular array with three layers.

In these simulations, it is observed that the two-plane arrays with equal lateral areas have less RMSE than the three-plane ones. Furthermore the rotated arrays with the same geometry have less RMSE than the normal arrays. So in sum the two-plane rotated triangular array has the best performance among these geometries. One can observe that as in the computation of the RMSE we have combined the effects of the azimuth and the elevation errors, given the fact that the azimuth angle is between 0 and 360° and the elevation angle is limited between −90 and 90°, the effect of the azimuth error would be more significant with respect to the elevation error in RMSE. In the two-plane arrays (with equal lateral area) the azimuth angle is better resolved (as the radius of the array is larger). In the three-plane arrays (with equal lateral area) the height is larger and consequently the elevation angle is better resolved. As such in sum the two-plane arrays have a better total resolution as observed in the simulations. For the case of equal lateral area and equal number of elements the arrays with triangular cross sections have less mean error with respect to the circular ones.

4. Conclusion

In this study, different 3D geometries of dipole arrays were investigated for two dimensional DOA determination in presence of mutual coupling and noise. In this process the MUSIC algorithm's search vector was modified by the normalized mutual impedance matrix and consequently a new pseudospectrum function was obtained. This method was examined for the cylindrical arrays and the rotated cylindrical arrays in a realistic situation (mutual coupling included) using half-wave dipole antennas and their performance was compared with the ideal arrays, using isotropic elements. It is noteworthy that a practical array of dipole antennas would have lower resolution near the array's zenith. The efficiency of the proposed method was examined with 3D antenna geometries for two dimensional (both azimuth and elevation angles) direction finding in presence of mutual coupling effect. The accuracy of the method was evaluated using RMSE estimation. Monte-Carlo simulations showed that in general dipole arrays (mutual

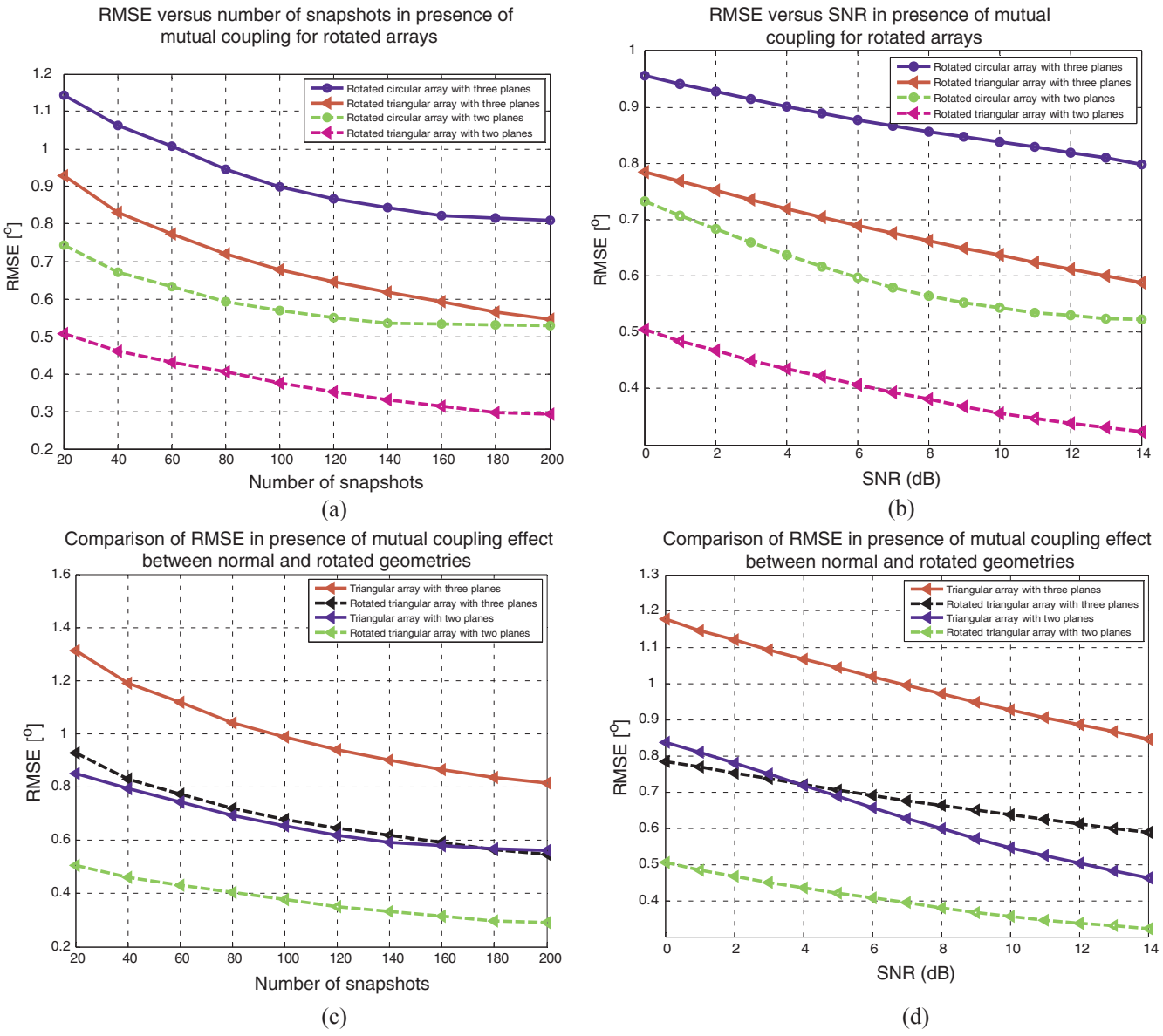

Fig. 9. Comparison of RMSE in different array geometries (normal and rotated). (a) RMSE versus number of snapshots for rotated geometries (triangular and circular) at fixed SNR = 7 dB. (b) RMSE versus SNR for rotated geometries (triangular and circular) at fixed number of snapshots (L = 100). (c) RMSE versus number of snapshots for normal and rotated geometries with triangular cross sections and equal number of antennas (at fixed SNR = 7 dB). (d) RMSE versus SNR for normal and rotated geometries with triangular cross sections and equal number of antennas (at fixed number of snapshots, L = 100).

Table 3
The average of estimation error for Fig. 9a.

Geometry	Average of estimation error (°)
Rotated circular with three planes	0.916
Rotated triangular with three planes	0.685
Rotated circular with two planes	0.583
Rotated triangular with two planes	0.391

Table 4
The average of estimation error for Fig. 9b.

Geometry	Average of estimation error (°)
Rotated circular with three planes	0.871
Rotated triangular with three planes	0.680
Rotated circular with two planes	0.595
Rotated triangular with two planes	0.374

coupling accounted for) have less resolution than the identical ideal isotropic arrays. In comparisons of 3D cylindrical array geometries (with the same number of elements and the same lateral areas) the arrays with less height and larger cross sectional areas have better resolution than their counterpart with larger height and less cross sectional area. Furthermore the cylindrical array with triangular cross section has a better resolution than the cylindrical array with circular cross section (with the same lateral areas and the same number of elements).

A novel geometry was proposed in which the cross sectional areas were rotated with respect to each other. Through Monte-Carlo simulations these new geometries showed better resolution than the conventional cylindrical geometries (with the same number of elements and the same cross sections). The rotation of the cylindrical geometries cross sections can be devised as a method of mitigation of the mutual coupling effect in these type of arrays as it was demonstrated in the simulation results.

Appendix A. Supplementary material

Supplementary data associated with this article can be found, in the online version, at http://dx.doi.org/10.1016/j.aeue.2017.12.019.

References

[1] Oumar OA, Siyau MF, Sattar TP. Comparison between MUSIC and ESPRIT direction of arrival estimation algorithms for wireless communication systems. In: The first international conference on future generation communication technologies; 2012. p. 99–103. http://dx.doi.org/10.1109/FGCT.2012.6476563.

[2] Gupta I, Ksienski A. Effect of mutual coupling on the performance of adaptive arrays. IEEE Trans Antennas Propag 1983;AP-31(5):785–91.

[3] Yeh C-C, Leou M-L, Ucci DR. Bearing estimations with mutual coupling present. IEEE Trans Antennas Propag 1989;37(10):1332–5. http://dx.doi.org/10.1109/8.43546.

[4] Friedlander B, Weiss AJ. Direction finding in the presence of mutual coupling. IEEE Trans Antennas Propag 1991;39(3):273–84. http://dx.doi.org/10.1109/8.7632.

[5] Dandekar KR, Xu G. Effect of mutual coupling on direction finding in smart antenna applications. Electron Lett 2000;36(22):1889–91.

[6] Su T, Dandekar K, Ling H. Simulation of mutual coupling effect in circular arrays for direction-finding applications. Microw Opt Technol Lett 2000;26(5):331–6. doi:10.1002/1098-2760(20000905)26:5 < 331::AID-MOP17 > 3.0.CO;2-M.

[7] Omar MMM, Kir A. The mutual coupling effect on the MUSIC algorithm for direction of arrival estimation. Int J Comput Appl 2011;35(4):36–40.

[8] Adve RS, Sarkar TK. Compensation for the effects of mutual coupling on direct data domain adaptive algorithms. IEEE Trans Antennas Propag 2000;48(1):86–94. http://dx.doi.org/10.1109/8.827389.

[9] Hui HT. Improved compensation for the mutual coupling effect in a dipole array for direction finding. IEEE Trans Antennas Propag 2003;51(9):2498–503. http://dx.doi.org/10.1002/anie.201408347.

[10] Lin M, Luxi Y. Blind calibration and DOA estimation with uniform circular arrays in the presence of mutual coupling. IEEE Antennas Wirel Propag Lett 2006;5:315–8. http://dx.doi.org/10.1109/LAWP.2006.883953.

[11] Dehmollain M, Hojjat N, Safavi-Naeini S, Jamali H. Simulation and compensation of antenna array mutual coupling effects on the performance of 2-d MUSIC algorithm. In: IEEE Antennas and Propagation Society International Symposium. Digest., Columbus: IEEE; 2003. p. 900–3.

[12] Goossens R, Rogier H. A hybrid UCA-RARE/Root-MUSIC approach for 2-D direction of arrival estimation in uniform circular arrays in the presence of mutual coupling. IEEE Trans Antennas Propag 2007;55(3):841–9. http://dx.doi.org/10.1016/j.aeue.2007.03.018.

[13] Ye Z, Liu Chao. 2-D DOA estimation in the presence of mutual coupling. IEEE Trans Antennas Propag 2008;56(10):3150–8. http://dx.doi.org/10.1109/TAP.2008.929446.

[14] Goossens R, Rogier H. Direction-of-arrival and polarization estimation with uniform circular arrays in the presence of mutual coupling. AEU – Int J Electron Commun 2008;62:199–206. http://dx.doi.org/10.1016/j.aeue.2007.03.018.

[15] Jiang G, Dong Y, Mao X, et al. Improved 2D direction of arrival estimation with a small number of elements in UCA in the presence of mutual coupling. AEU - Int J Electron Commun 2016;71:131–8. http://dx.doi.org/10.1016/j.aeue.2016.10.012.

[16] Poormohammad S, Farzaneh F. Precision of direction of arrival (DOA) estimation using novel three dimensional array geometries. AEU - Int J Electron Commun 2017;75:35–45. http://dx.doi.org/10.1016/j.aeue.2017.02.013.

[17] Kraus J. Antennas. 2nd ed. New Delhi: Tata McGraw-Hill; 1997.